MOLECULAR AND CELLULAR BIOLOGY, May 2010, p. 2229–2240 Vol. 30, No. 9
0270-7306/10/$12.00 doi:10.1128/MCB.00723-09

p27^{kip1} Controls Cell Morphology and Motility by Regulating Microtubule-Dependent Lipid Raft Recycling▽†

Barbara Belletti,[1] Ilenia Pellizzari,[1] Stefania Berton,[1] Linda Fabris,[1] Katarina Wolf,[2] Francesca Lovat,[1]‡ Monica Schiappacassi,[1] Sara D'Andrea,[1] Milena S. Nicoloso,[1]§ Sara Lovisa,[1] Maura Sonego,[1] Paola Defilippi,[3] Andrea Vecchione,[4] Alfonso Colombatti,[1,5] Peter Friedl,[2] and Gustavo Baldassarre[1]*

Division of Experimental Oncology 2, Centro di Riferimento Oncologico, National Cancer Institute, Aviano 33081, Italy[1]; Microscopical Imaging of the Cell, Department of Cell Biology, NCMLS, Radboud University, Nijmegen Medical Centre, 6500 HB Nijmegen, Netherlands[2]; Molecular Biotechnology Center, University of Torino, Turin, Italy[3]; Division of Pathology, II University of Rome La Sapienza, Ospedale Santo Andrea, Rome, Italy[4]; and Dipartimento di Scienze e Tecnologie Biomediche and MATI Center of Excellence, University of Udine, 33100 Udine, Italy[5]

Received 4 June 2009/Returned for modification 20 July 2009/Accepted 16 February 2010

p27^{kip1} (p27) is an inhibitor of cyclin/cyclin-dependent kinase complexes, whose nuclear loss indicates a poor prognosis in various solid tumors. When located in the cytoplasm, p27 binds Op18/stathmin (stathmin), a microtubule (MT)-destabilizing protein, and restrains its activity. This leads to MT stabilization, which negatively affects cell migration. Here, we demonstrate that this p27 function also influences morphology and motility of cells immersed in three-dimensional (3D)matrices. Cells lacking p27 display a decrease in MT stability, a rounded shape when immersed in 3D environments, and a mesenchymal-amoeboid conversion in their motility mode. Upon cell contact to extracellular matrix, the decreased MT stability observed in p27 null cells results in accelerated lipid raft trafficking and increased RhoA activity. Importantly, cell morphology, motility, MT network composition, and distribution of p27 null cells were rescued by the concomitant genetic ablation of Stathmin, implicating that the balanced expression of p27 and stathmin represents a crucial determinant for cytoskeletal organization and cellular behavior in 3D contexts.

The importance of developing and utilizing three-dimensional (3D) models to understand the molecular and cellular signaling events underlying *in vivo* biology is becoming increasingly clear and critical, especially in cancer (50). To spread into surrounding tissues and metastasize, tumor cells need to increase their invasive potential, rearrange their cytoskeleton, and remodel the extracellular matrix (ECM) (39). It has been proposed that internal cytoskeletal dynamics and cellular morphology can influence the environment recognition and subsequent choice of motility mode through the ECM, where cells with elongated protrusions preferably move using a mesenchymal motility while more rounded cells rather invade using an amoeboid-like motility program (17). Mesenchymal migration employs more stringent, focalized cell-matrix interactions and Rac-driven protrusions and causes proteolytic ECM remodeling, whereas amoeboid cell movement lacks focalized cell-ECM interactions and is Rho/ROCK dependent, and cells progress by squeezing their body rather than by ECM degradation (38). Because they depend upon 3D interactions with the surrounding tissue, these processes can hardly be investigated in standard 2D culture conditions, where intracellular signaling pathways directing cell polarity, proliferation, and differentiation are orchestrated in profoundly different ways (17). Over the last few years, many proteins have been implicated in the control of 2D versus 3D motility. Among others, RhoA and its ubiquitin ligase Smurf1 have been demonstrated to act in distinct ways whether cell motility is explored by 2D tissue culture assay or by 3D and *in vivo* models, and their roles during the migration process may greatly differ depending on the cellular state and context (37, 38, 45).

p27^{kip1} (hereafter p27) is a cell cycle inhibitor that has been implicated in the regulation of cell motility (2, 4, 6). We previously demonstrated that in early steps of cell adhesion to ECM or when cells are immersed in 3D matrices, p27 translocates to the cytoplasm, where it binds and inhibits stathmin, a microtubule (MT)-destabilizing protein (2). In the absence of p27, including when it has been knocked down or degraded in tumors, a decrease in MT stability is then responsible for increased motility and invasive potential of cells (2). On the other hand, other reports have shown that absence of p27 impairs motility of cells when tested in 2D assays, such as wound healing or random motility (6), thus suggesting that the roles of p27 may be different, depending on cellular contexts.

It is well known that MTs are necessary for directional motility and provide a polarized network to allow organelle and protein movements throughout the cell (47). This trafficking is essential for receptor and integrin recycling, which, in turn, is

* Corresponding author. Mailing address: Division of Experimental Oncology 2, Centro di Riferimento Oncologico, National Cancer Institute, Via Franco Gallini, 2, 33081 Aviano, Italy. Phone: 39 0434 659 233. Fax: 39 0434 659 428. E-mail: gbaldassarre@cro.it.

† Supplemental material for this article may be found at http://mcb.asm.org/.

‡ Present address: Department of Molecular Virology, Immunology & Medical Genetics Comprehensive Cancer Center, Ohio State University, Columbus, OH.

§ Present address: Experimental Therapeutics, The University of Texas M.D. Anderson Cancer Center, Houston, TX 77030.

▽ Published ahead of print on 1 March 2010.

required for migration (43). Rho GTPases, key regulators of cell migration, also affect the microtubule cytoskeleton during directed migration, contributing to its stabilization at the leading edge (at least in part through stathmin inhibition) and to the repositioning of the microtubule organizing center (MTOC) (14, 36). In turn, MTs can modulate Rho GTPase activity, with MT outgrowth activating Rac1 and MT disruption activating RhoA, although the molecular mechanism of these regulations under physiological and pathological conditions is not completely understood (11, 43, 47).

Interestingly, Rho GTPase activity has been shown to be negatively regulated by p27 during 2D migration (6), thus suggesting that cross talk among these different molecules and signaling pathways must exist to appropriately coordinate and fulfill complex cellular functions, such as migration, invasion, and division.

Here, we demonstrate that p27 regulates lipid raft trafficking and Rho GTPase activity via its interaction with stathmin and that this molecular pathway is probably involved in the control of cell morphology and motility in 3D environments.

MATERIALS AND METHODS

Cell culture, retroviral transduction, and PCR on genomic DNA. 3T3 fibroblasts and mouse embryonic fibroblasts (MEFs) were cultured in Dulbecco's modified Eagle's medium (DMEM) supplemented with 10% fetal bovine serum (FBS; Sigma). Primary wild-type (WT), p27 knockout (KO), and p27/stathmin DKO MEFs were prepared from embryos at day 13.5, according to standard procedures. Primary MEFs (at least five different preparations/genotype) were used between passages 3 and 5 without significant differences. The correct genotype of WT, p27 KO, and p27/stathmin DKO cells, was determined by PCR, as described previously (2, 16). 3T3 fibroblasts were obtained from primary MEFs following the 3T3 immortalization protocol. Cell clones of 3T3 p27 WT or KO stably expressing stathmin and 3T3 p27 KO stably expressing p27 or the empty vectors were obtained by retroviral transduction with a vector carrying puromycin resistance (murine stem cell virus retroviral vectors; Clontech), following the manufacturer's instructions. 293T/17 cells (ATCC CRL-11268) used to produce retroviruses were grown in DMEM supplemented with 10% FBS (Sigma).

Caveolin 1-silenced p27 KO cells were generated using two different shRNAs against mouse caveolin 1 from the MISSION library (TRCN0000112662 and TRCN0000112664; SigmaAldrich) (32), using either transient or stable (puromycin-selected) lentiviral transduction, with no significant differences (data not shown, but see Fig. 6, below). In the same cells, the nontarget sh-control vector (SHC202; SigmaAldrich) has been used as control.

Proliferation assays. Proliferation was assessed by 3-(4,5-dimethyl-2-thiazolyl)-2,5-diphenyl-2H-tetrazolium bromide assay (Sigma) or by fluorescence-activated cell sorting analysis, as described in references 2 and 3.

Adhesion and migration assays. For adhesion experiments, cells were starved overnight in DMEM–0.1% FBS and then detached and seeded onto dishes coated with fibronectin (FN; 10 μg/ml; Sigma). Where indicated, paclitaxel (Taxol; 100 nM; TEVA), C3-exoenzyme (2 ng/ml; Cytoskeleton), and Y27632 (10 μM; Calbiochem) were added during adhesion. To differentially extract soluble and polymerized protein fractions, at indicated times cells were scraped at room temperature in MT-stabilizing buffer [MSB; 85 mM piperazine-*N*,*N*′-bis(2-ethanesulfonic acid) (PIPES; pH 6.5), 1 mM EGTA, 1 mM $MgCl_2$, 2 M glycerol, 0.5% Triton X-100, 4 μg/ml paclitaxel, and protease inhibitors) or at 4°C in NP-40 lysis buffer for total lysates (2). Haptotaxis was performed by labeling cells with DiI fluorescent vital dye (Molecular Probes) and plating 1×10^5 cells in the upper chamber of transwell-like inserts, carrying a fluorescence-shielding porous polyethylene terephthalate membrane with 0.8-μm pores (HTS FluoroBlok; BD) previously coated on the underside with FN (20 μg/ml) or collagen I (20 μg/ml; BD), as indicated. The time-dependent migratory behavior of the cells was monitored by using a SPECTRAFluor Plus microplate fluorometer, as described previously (2). The quantitative cell adhesion assay (centrifugal assay for fluorescence-based cell adhesion [CAFCA]) used in this study has been previously described (2).

Time-lapse microscopy. Time-lapse microscopy and cell tracking analyses were performed as previously described (49). Briefly, cells were detached and suspended in a buffered collagen I solution, pH 7.4, at 1.67 mg/ml final concentration (Vitrogen). The suspension was allowed to polymerize for 30 min at 37°C in a 5% CO_2 atmosphere in a self-constructed 3D chamber and then overlaid with serum-free medium (SFM). Pictures/images were collected every 4 min for 18 h using a charge-coupled-device camera mounted onto the microscope. Collected images were used to create a movie (10 images per second) and analyzed with a custom cell-tracking software to collect different locomotion parameters (26). In brief, 40 cells were randomly selected and their *x*-*y* coordinates were obtained for each step (12-min step interval), and the total distance and the steady state as well as average cell speed were obtained for each cell of the population.

Morphology in 3D and evasion assay. For the evaluation of cellular morphology in 3D matrices, cells were included in Matrigel (6 mg/ml; BD) or collagen I (1.7 mg/ml; BD or Vitrogen) 10-μl drops on a coverslip (7.5×10^5 cells/ml) and maintained for 1 h upside down at 37°C, to allow collagen I polymerization. Then, complete medium or serum-free medium was added, as indicated. Drops were incubated for the indicated times (6 to 8 h) and photographed using a phase-contrast microscope to evaluate cell morphology. When indicated, cytochalasin D (0.5 μM; Sigma), nocodazole (1 μM; Sigma), C3-exoenzyme (2 ng/ml; Cytoskeleton), or Y27632 (10 μM; Calbiochem) was added to the Matrigel or collagen mix to include the cells and to the medium. In some cases, the shapes of single cells immersed in 3D matrices were calculated by sorting them as round (no dominant pseudopod), elongated (one to two protrusions), or stellate (more than two protrusions). Evasion assays were set up in the same way, except that cell drops were plated on plastic multiwell plates and evasion ability was estimated 4 days after inclusion. Cells outside each drop (5 drops/cell line/experiment) were counted to estimate the evasion ability of each cell line. The evasion ability was also estimated by measuring the distance covered by crystal violet-stained cells 10 days after inclusion.

Immunofluorescence analysis. For immunofluorescence staining, cells were immersed in Matrigel or collagen I drops on coverslips for the indicated times and fixed in phosphate-buffered saline (PBS)–4% paraformaldehyde (PFA) at room temperature (RT), permeabilized in PBS–0.2% Triton X-100, and blocked in PBS–1% bovine serum albumin (BSA) or 10% normal goat serum. Incubation with primary antibodies (anti-α-tubulin–fluorescein isothiocyanate [FITC] and anti-acetylated tubulin [Sigma]; pS3-cofilin [Cell Signaling]; RhoA [Upstate]) was performed overnight at 4°C in PBS–1% BSA or 1% normal goat serum, and then samples were washed in PBS and incubated with secondary antibodies (Alexa Fluor 488-, 546-, or 633-conjugated anti-mouse or anti-rabbit antibodies; Invitrogen) for 1 h at RT. In some cases antibody incubation was followed by staining of F-actin with phalloidin-tetramethyl rhodamine isocyanate or Alexa Fluor 647 or Alexa Fluor 546 (Invitrogen) for 30 min at RT, by nuclear staining with 1 μg/ml Hoechst 33258 in PBS for 10 min at RT, or with 1 μM Sytox Green (Invitrogen) for 30 min at RT. Stained cells were then observed using a confocal laser-scanning microscope (TSP2 Leica) interfaced with a Leica DMIRE2 fluorescence microscope. Images were acquired using a Nikon Diaphot 200 epifluorescence microscope equipped with distinguishing filters.

Tubulin dilution assay. The tubulin dilution assay was performed essentially as described previously (2), with some modifications due to the inclusion of the cells in 3D matrices. Briefly, cells included in 3D collagen I for 4 h were incubated in PEM buffer (80 mM PIPES, 1 mM $MgCl_2$, 1 mM EDTA) containing 0.2% Triton X-100 for 2 min at 37°C and then washed and incubated in PEM buffer for 10 min at 37°C. Free tubulin heterodimers are in this way washed out of the cells, allowing distinctions between dynamic and stable MT. Cells were then fixed in PBS–4% PFA and processed for immunofluorescence analysis, as described above.

Immunoblotting analysis. Western blot (WB) analyses were performed as previously described (2). In some cases, revelation of signal was performed with enhanced chemiluminescence (ECL) and in others with Odyssey infrared (IR) imaging (LI-COR). Primary antibodies were purchased from Sigma (for α-tubulin, acetylated α-tubulin, Op18/stathmin, and actin), Santa Cruz Biotechnology (vinculin and RhoA), BD Transduction Laboratories (stathmin/metablastin, p27, cofilin, and caveolin) Upstate (RhoA), and Cell Signaling (pSer3 cofilin). Secondary horseradish peroxidase-conjugated antibodies were from Amersham; secondary IR-conjugated antibodies were from Invitrogen (Alexa Fluor 680) and from Rockland (IRDye 800).

Wound healing assay. Exponentially growing cells (4×10^5) were plated in wells of a six-well plate to create a dense monolayer and then scratched with a yellow tip. Complete medium was added after washing in PBS, and wound closure was monitored over the time. After 24 h pictures were taken to calculate and compare the cellular capacity for closing the scratch.

RhoA activity assay. Exponentially growing MEFs (between passages 3 and 5) were incubated in serum-reduced medium (0.1% FBS–DMEM) overnight and

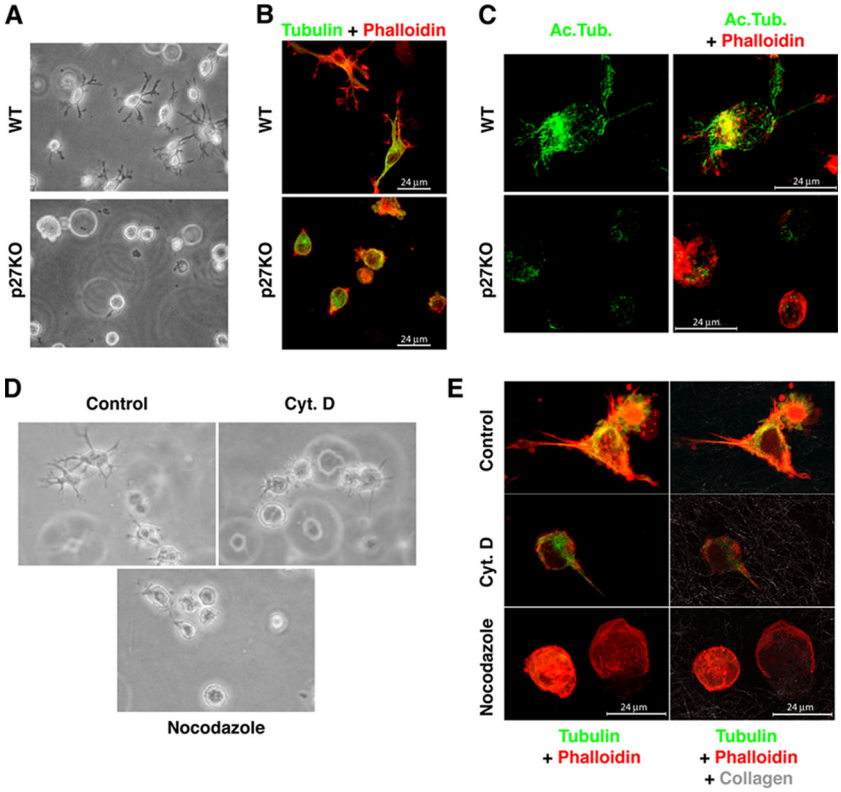

FIG. 1. p27 controls cellular morphology through regulation of the MT network. (A) Phase-contrast microscopy of WT or p27 KO 3T3 fibroblasts immersed in a 3D collagen I matrix for 6 h. A typical image is shown, and a 10× objective was used. (B) Immunofluorescence analysis of α-tubulin (FITC; green) and F-actin (phalloidin; red) in WT or p27 KO MEFs immersed in a 3D collagen I matrix for 6 h. A typical image acquired by confocal microscopy is shown. (C) Immunofluorescence analysis of acetylated tubulin (green) and F-actin (phalloidin; red) in WT or p27 KO MEFs immersed in a 3D collagen I matrix for 4 h and subjected to a tubulin dilution assay prior to fixation. A typical image of a 3D confocal reconstruction is shown. (D) Phase-contrast microscopy of p27 KO MEFs immersed in a 3D collagen I matrix for 6 h (control), in the presence of 0.5 μM cytochalasin D (Cyt. D) or 1 μM nocodazole. A typical image is shown, and a 20× objective was used. (E) Immunofluorescence analysis of α-tubulin (FITC; green), F-actin (phalloidin; red), and collagen fibers (reflection; gray) in p27 KO MEFs treated as for panel D. Typical images of 3D confocal reconstructions (left panels) and of a single confocal section (right panels) of the same fields are shown.

then stimulated with 25 ng/ml basic fibroblast growth factor (bFGF; Calbiochem) for 5 and 10 min. In other experiments, MEFs were incubated in SFM (0.1% BSA–DMEM) for 24 h and then detached and kept in suspension in SFM for 30 min at 37°C. Then cells were adhered to FN-coated dishes (25 μg/ml; Sigma) for 15 to 30 to 60 min. At the indicated time points, cells were lysed and at least 2 mg of protein was tested in a pulldown assay with glutathione *S*-transferase (GST)–mDIA rhotekin binding domain fusion protein bound to glutathione-Sepharose high performance (GE Healthcare) for 1 h at 4°C, as previously reported (12). After thorough washes, the samples were boiled for 10 min in Laemmli buffer to detach active GTP-bound Rho and then loaded on 12.5% SDS-PAGE gels (Criterion; Bio-Rad) and immunoblotted using an anti-RhoA antibody.

Lipid raft trafficking. The lipid raft trafficking assay was carried out essentially as previously described by others (1). Briefly, for the internalization assay, adherent cells were placed on ice for 15 min and then incubated for an additional 15 min with 2 μg/ml Alexa Fluor 488- or Alexa Fluor 594-cholera toxin B (CTxB; Invitrogen) in PBS. Cells were then detached, held in suspension 5 to 60 min, cytospun, and fixed in PBS–4% PFA for 20 min at RT. For time-lapse analysis, cells were treated as above but immediately after detachment were dispensed onto poly-HEMA-coated glass-bottom dishes (Willco wells) to be examined with a confocal microscope. Images were taken every 30 s for 10 min. When paclitaxel was used, cells were pretreated for 2 h with 10 or 100 nM paclitaxel and then labeled and treated as above, always in the presence of paclitaxel. To evaluate recycling of lipid rafts to the cellular membrane, cells were labeled as above and then detached and held in suspension for 1 h. Cells were then washed and plated onto FN-coated coverslips for 30 to 60 min and then fixed in PBS–4% PFA for 20 min at RT. Nuclei were counterstained using 1 μM Sytox Green (Invitrogen) for 20 min at RT. Coverslips were mounted in Mowiol 4-88 (Calbiochem) with 2.5% 1,4-diazabicyclo(2,2,2)octane (Sigma) and observed using a confocal laser-scanning microscope (TSP2 Leica) interfaced with a Leica DMIRE2 fluorescence microscope. Fluorescent signal was quantified using the Leica LAS software.

RESULTS

p27 controls cellular morphology through regulation of the MT network. p27 null 3T3 fibroblasts display an enhanced motility when challenged in matrix-based migration assays (2). Concomitantly, we also observed that they displayed a different morphology from their WT counterpart when immersed in 3D matrices, since they failed to form long cellular protrusions and, conversely, assumed an overall rounded shape (Fig. 1A). This observation was also confirmed on primary MEFs, demonstrating that the different shape acquired in 3D is not due to clonal selection (see Fig. S1B and C in the supplemental material). The immunofluorescence analysis of α-tubulin in fibroblasts immersed in 3D collagen I showed that the MT network was differently organized in the presence or absence of p27. MTs were well distributed throughout the cell body and inside the protrusions in the WT cells, while they remained located perinuclearly in the p27 KO cells (Fig. 1B). Under the same

conditions, the actin cytoskeleton exhibited a peripheral distribution in both fibroblasts (Fig. 1B). To ascertain whether in 3D MT stability was affected by p27 loss, we performed a tubulin dilution assay, in which free tubulin dimers are allowed to flow out of the cell *in vivo* and only stable MTs are retained, and this is coupled with immunofluorescence analysis with an antibody directed against acetylated tubulin, which identifies the pool of more stable MT in the cell. Results demonstrated that the different intracellular distribution of MT in p27 KO cells was accompanied by a significant decrease in the pool of stable MT (Fig. 1C). To test whether the different morphology was dependent on a diverse cytoskeletal organization or whether, on the contrary, the cytoskeletal diversity was only a consequence of the morphological phenotype, we used low doses of different drugs that specifically affect the actin or the tubulin networks. Treatment of WT cells with 0.5 μM cytochalasin D (an actin-disrupting drug) did not abrogate the formation of cellular protrusions, although they appeared to be shorter than those of control cells (Fig. 1D and E). Conversely, destabilizing the MT network by using low doses of nocodazole (1 μM) strongly affected the abilities of fibroblasts to assume their typical mesenchymal shape, as displayed in both phase-contrast and immunofluorescence images of the cells within the 3D collagen I matrix (Fig. 1D and E). The results were confirmed by time-lapse video microscopy, which showed that WT cells immersed in 3D collagen I started to form protrusions within 2 h of inclusion (see Video S1 in the supplemental material). Cytochalasin D retarded but did not abolish this process, although it completely inhibited cell movements (see Video S2). On the contrary, treatment with low doses of nocodazole prevented protrusion formation and consistently increased cell motility (see Video S3), closely resembling the phenotypes of p27 KO cells (see Video S7). These results suggested that the MT network plays an important role in the acquisition of proper cellular morphology in 3D matrices and that this process is altered in p27 KO cells.

We previously demonstrated that p27 participates in the control of cell motility by interfering with the MT-destabilizing activity of stathmin (2) and that stathmin activity plays a pivotal role in the acquisition of a rounded cell shape in 3D environments (3). To verify that the p27-stathmin interaction is able to regulate fibroblast cellular morphology in 3D contexts, several stable cell clones were generated. Results showed that clonal selection *per se* (via transfection with an empty vector) did not alter the morphology or the motility of parental 3T3 p27 WT and KO fibroblasts (see Fig. S2 in the supplemental material), and reexpression of p27 WT in p27 null fibroblasts resulted in a rescue of the morphological and motile phenotypes of p27 null cells (see Fig. S3A, B, and F). In accord with the hypothesis that an unbalanced expression ratio between p27 and stathmin underlies the observed phenotypes in p27 KO cells, increasing the stathmin levels in WT fibroblasts resulted in the acquisition of a rounded cell shape in a 3D context, coupled with an increased cell speed (see Fig. S3C, D, and E), thus mimicking key features of p27 null cells. It is noteworthy that overexpression of stathmin in p27 KO cells did not alter their 3D phenotypes (see Fig. S3 and S5), nor did it affect the proliferation rate or 2D shape and motility (see Fig. S4) in either WT or p27 KO fibroblasts.

Altogether, these results demonstrate that the p27/stathmin expression ratio represents an important determinant for mouse fibroblast morphology and motility in 3D contexts, and this is accomplished through the regulation of MT dynamics.

Generation and characterization of p27/stathmin DKO MEFs. To better address the role of stathmin in the phenotype of cells lacking p27 expression, we generated p27/stathmin DKO mice by intercrossing mice heterozygous for both genes. PCR of embryo genomic DNA and WB analysis on fibroblast lysates confirmed the correct genotypes of derived MEF populations (data not shown, but see Fig. S6A in the supplemental material). Phase-contrast microscopy images showed that DKO MEFs displayed a similar morphology to the other genotypes under standard culture conditions (see Fig. S6B, upper panels). Also, motility in 2D did not differ from that exhibited by WT and p27 KO MEFs (see Fig. S6C), thus implying that the cell machinery necessary for 2D migration was not significantly affected by simultaneous ablation of p27 and stathmin. Then, we included MEFs from the different genotypes into 3D matrices either in complete medium (CM) or in SFM and observed their morphologies at different time points (see Fig. S6B, middle and lower panels). Alternatively, MEFs were included in collagen I drops and monitored over time until they exited from the drop (see Fig. S6E), or they were tested for haptotaxis in collagen I-coated transwells (see Fig. S6D). Results showed that, under all conditions considered, DKO MEFs behaved in a very similar manner to WT MEFs. They acquired an elongated shape with multiple extensions protruding in the 3D matrix, evaded the collagen I drop to a lesser extent than the fibroblasts with only p27 knocked out, and migrated comparable to WT cells in collagen I-coated transwells. Thus, the results from the double knockout model indirectly confirmed that, also in the 3D environment, the migratory advantage and morphological features of p27 KO cells are due to increased stathmin activity.

Stathmin loss counteracts the altered MT stability of p27 KO cells. To evaluate whether and how the composition of the cytoskeletal network of the DKO cells could account for the rescue of the morphological and migratory phenotypes of p27 KO cells, we performed immunofluorescent staining of the actin and MT networks in MEFs in a 3D collagen I matrix, following the tubulin dilution assay. Tubulin staining of DKO fibroblasts revealed MT localization in the cellular protrusions and colocalization with the actin cytoskeleton, in a configuration very similar to that of the WT MEFs (Fig. 2A). In particular, examination of pseudopods and filopodia extending from the cell body revealed the presence of MT until the very end of those protrusions in WT and DKO MEFs and attested to the different arrangements in the p27 KO cells. Again, these latter fibroblasts appeared much more rounded and their protrusions, where present, were shorter and filled only with actin fibers, reinforcing the idea that MT organization is defective in these cells. To better characterize the differences in MT stability in these cells, we stained the cells using an antibody directed against acetylated tubulin, which marks and identifies the pool of more stable MTs in the cell. As expected, p27 KO MEFs displayed a marked decrease of stable MT, while WT and DKO MEFs exhibited marked staining for stable MT, both in the cell body and in the protrusions (Fig. 2B). As a complementary approach, the stability of MT in the MEFs of different genotypes was evaluated following adhesion to ECM. Adhe-

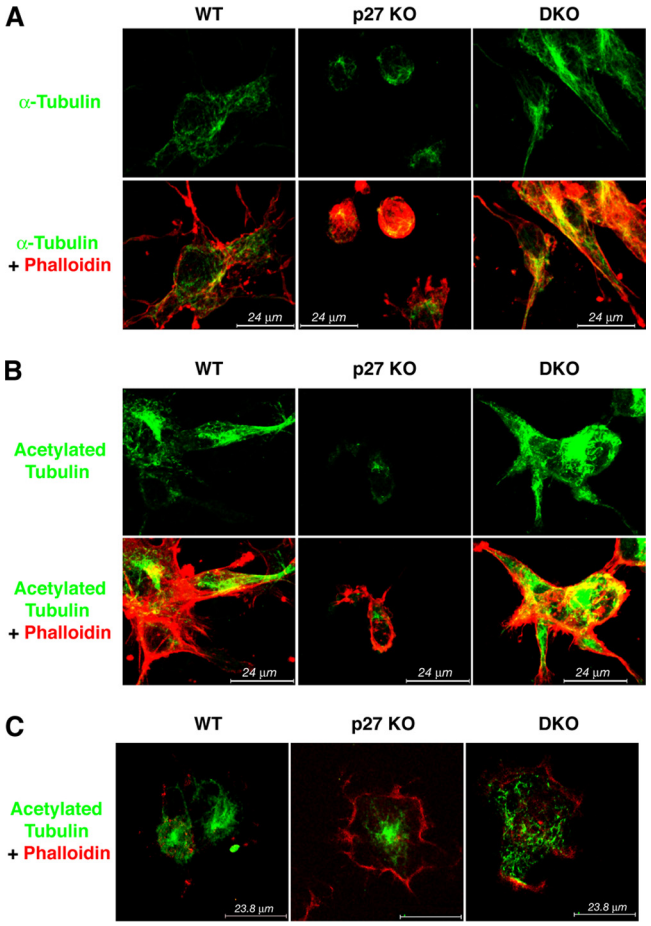

FIG. 2. DKO MEFs display normal MT organization in a 3D context. (A) Immunofluorescence analysis of α-tubulin (FITC; green) and F-actin (phalloidin, red) in WT, p27 KO, and DKO MEFs immersed in a 3D collagen I matrix for 6 h and subjected to the tubulin dilution assay prior to fixation. A typical image acquired by confocal microscopy is shown. (B) Immunofluorescence analysis of acetylated tubulin (green) and F-actin (phalloidin; red) in WT, p27 KO, and DKO MEFs immersed in a 3D collagen I matrix for 6 h. A typical image acquired by confocal microscopy is shown. (C) Immunofluorescence analysis of acetylated tubulin (green) and F-actin (phalloidin; red) in WT, p27 KO, and DKO MEFS alowed to adhere to collagen I for 30 min. Cells were fixed in methanol-acetone to allow outflow of soluble proteins. A typical image acquired by confocal microscopy is shown.

sion *per se* was not affected by loss of p27, stathmin, or both (see Fig. S7A in the supplemental material), but differential extraction of soluble and polymerized protein fractions from cells adhered to fibronectin provided evidence that the decrease of stable MT content in p27 KO MEFs was rescued by DKO MEFs (see Fig. S7B). This result was then confirmed using 3T3 fibroblasts and another marker of stable MT, detyrosinated tubulin (see Fig. S7C). Finally, cells were adhered to collagen I and then fixed in methanol-acetone to allow the outflow of soluble tubulin dimers. Immunofluorescence analysis of acetylated tubulin corroborated the WB results, showing reduced staining for stable MT in p27 KO MEFs while DKO and WT fibroblasts displayed similar levels of acetylated MT (Fig. 2C). Altogether, these results indicate that balanced expression and activity of p27 and stathmin are required for correct MT stability, and this, in turn, is necessary for acquiring the typical mesenchymal morphology and motility of wild-type fibroblasts in 3D contexts. However, the molecular mechanism by which these processes are accomplished was still to be clarified.

The rounded cell shape of p27 KO cells in 3D is associated with high RhoA activity. The rounded cell morphology and amoeboid motility in 3D environments have been linked to hyperactivation of the Rho pathway at the plasma membrane (38, 39). Interestingly, it has been reported that p27 can affect cell motility by altering either RhoA (6) or Rac1 (31) activities, and recent data also demonstrated that adhesion-dependent activation of small GTPases could be impaired by preventing MT assembly via high doses of nocodazole (1). Thus, we wondered whether the different expression ratios between p27 and stathmin in MEFs could modify the activation level of the Rho pathway, and we tested this hypothesis either after growth factor stimulation or after cell contact with ECM substrates. After stimulation with FGF, RhoA is more rapidly and strongly activated in p27 KO MEFs than in the WT counterpart (Fig. 3A), as previously reported by others (6). Next, we assayed RhoA activity in MEFs following adhesion to ECM at very early to late time points. As illustrated in Fig. 3B, p27 KO MEFs showed increased RhoA activity compared to WT cells at all considered adhesion times, with a peak of activity after 1 h of adhesion. Conversely, in WT MEFs RhoA activity reached its peak after 15 min, and then the activity gradually decreased (Fig. 3B). Importantly, RhoA activity in DKO cells exactly reproduced the pattern observed in WT MEFs (Fig. 3B). It is noteworthy that the effects observed were specifically due to pathways activated by cell-ECM contact, because when RhoA activity was evaluated in cells held in suspension, p27 KO MEFs displayed lower levels of active RhoA than WT or DKO cells. These results were also confirmed by WB analysis of phosphorylation levels of pS3 cofilin, a known target of the RhoA-ROCK1 pathway, following cell adhesion to the ECM component. The increase of pS3 cofilin levels observed in p27 KO MEFs after 30 and 60 min of cell adhesion was significantly higher than that in WT cells (Fig. 3C) and was completely abrogated by treatment of the cells with two specific inhibitors of the RhoA-ROCK1 pathway (C3 endotoxin and Y27632), both in p27 KO MEFs (Fig. 3D) and in p27 WT or DKO cells (data not shown). This confirmed that pS3 cofilin can be used as a measure of RhoA activation in our model system.

In order to verify whether an alteration of MT stability could specifically impinge on the Rho pathway, we first treated exponentially growing WT MEFs with low doses of nocodazole, aiming to decrease MT stability without completely destroying the MT cytoskeleton. This resulted in a dose-dependent increase in Ser3 cofilin phosphorylation, reaching a plateau at 0.1 μM nocodazole (Fig. 3E, upper panel), suggesting that cross talk between MT stability and the RhoA pathway existed also in our context. Then, we tested the same conditions in experiments of adhesion to ECM. In WT cells adhered to FN for 30 and 60 min, nocodazole treatment increased pS3 cofilin levels in a dose-dependent manner (Fig. 3E, lower panel). Then, as a reverse approach, p27 KO cells were treated with low doses of paclitaxel to increase the stability of their MT cytoskeleton. WB analysis of cells adhered to FN showed a complete abrogation of cofilin phosphorylation in the presence of paclitaxes

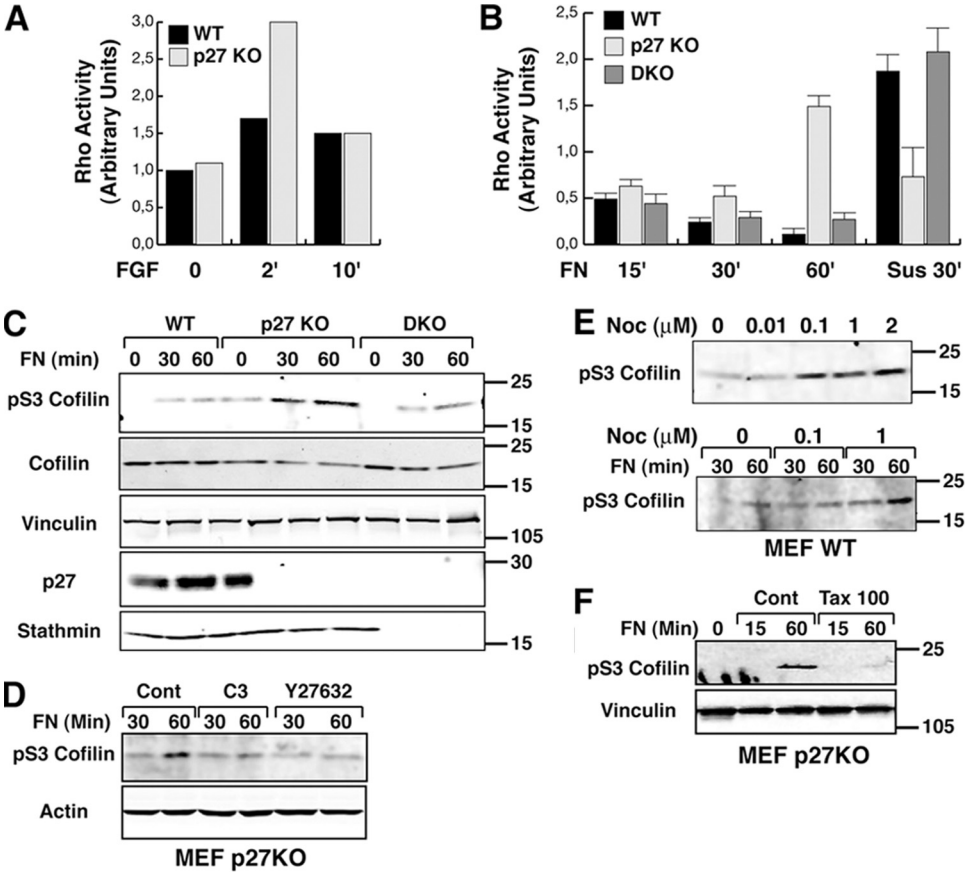

FIG. 3. Rho A activity is high in p27 KO cells following adhesion to ECM substrates. (A) Results of a pulldown assay of active RhoA in WT and p27 KO MEFs incubated in reduced serum (0.1%) medium overnight and then stimulated with bFGF (25 ng/ml) for the indicated times. (B) Results of a pulldown assay of active RhoA in WT, p27 KO, and DKO MEFs. Cells were serum starved for 24 h, detached, and kept in suspension for 30 min (Sus) and then adhered to FN (30 μg/ml) for the indicated times. Data represent the means of three independent experiments. (C) Western blot analysis of pSer3-cofilin on lysates from WT, p27 KO, and DKO MEFs alowed to adhere to FN (10 μg/ml) for the indicated times. Standard molecular weights are indicated on the right. Vinculin was used as a loading control. (D) Western blot analysis of pSer3-cofilin on lysates from p27 KO MEFs allowed to adhere to FN (10 μg/ml) for the indicated times in the presence of C3-exoenzyme (2 ng/ml) or Y27632 (10 μM). (E) Western blot analysis of pSer3-cofilin on lysates from WT MEFs treated with increasing doses of nocodazole (upper panel) or cells allowed to adhere to FN (10 μg/ml) for the indicated times in the presence of nocodazole at the indicated doses (lower panel). Standard molecular weights are indicated on the right. (F) Western blot analysis of pSer3-cofilin in lysates from p27 KO MEFs allowed to adhere to FN (10 μg/ml) for the indicated times in the presence of 100 nM paclitaxel. Standard molecular weights are indicated on the right.

(Fig. 3F). Altogether, these data suggest that p27 influences adhesion-dependent RhoA activity by regulating MT stability and that this effect is achieved by its interaction with stathmin, since it is reversed by simultaneous loss of the two proteins in the DKO model.

To validate these findings in a 3D environment, we evaluated the phosphorylation of Ser3 cofilin in p27 KO MEFs included in a 3D collagen I matrix by using immunofluorescence analysis. When included in the 3D collagen I, p27 KO MEFs displayed a significantly higher expression of pS3 cofilin (Fig. 4A). Computational analysis of the mean level of green fluorescence/cell demonstrated that the observed differences were highly statistically significant (mean intensity levels ± standard errors in arbitrary units were as follows: WT, 15 ± 7; p27 KO, 50 ± 12; DKO, 18 ± 9; $P < 0.0001$ between p27 KO and WT or DKO; P not significant between WT and DKO MEFs). Noticeably, treatment of p27 KO cells either with the C3-exoenzyme or with Y27632 not only resulted in the abrogation of cofilin phosphorylation (mean intensity levels 10 ± 4 and 8 ± 5 when the cells were treated with C3 or Y27632, respectively) but also in the acquisition of an elongated phenotype (Fig. 4B; see also Fig. S8A and B in the supplemental material). Altogether these data strongly support our hypothesis that alteration of RhoA activity is involved in the 3D morphological phenotype of p27 KO MEFs and that its differential activation is linked to the altered MT dynamics of these cells.

Impaired MT stability of p27 KO MEFs results in altered vesicular trafficking. At this point, we asked the question of how alterations of proper MT dynamics in our cellular model system could be responsible for modification of RhoA activity and, eventually, for morphological and motile transitions. Recently, Schwartz and coworkers demonstrated that MT dynamics control Rac1 activity following cell adhesion to ECM, impinging on lipid raft recycling (1). Lipid rafts represent membrane microdomains that segregate specific groups of pro-

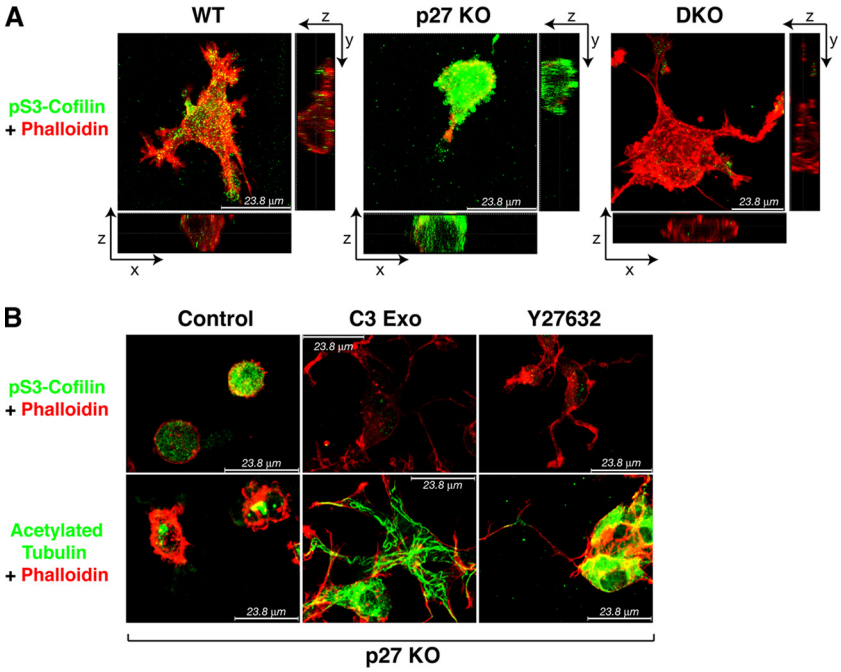

FIG. 4. Rounded cell shapes of p27 KO cells in a 3D matrix is associated with high RhoA activity. (A) Immunofluorescence analysis of pSer3-cofilin (green) and F-actin (phalloidin; red) in WT, p27 KO, and DKO MEFs immersed in a 3D collagen I matrix for 6 h. A typical image on the *x*, *y*, and *z* axes acquired by confocal microscopy is shown. (B) Immunofluorescence analysis of pSer3-cofilin (green) and F-actin (phalloidin; red) (upper panels) or acetylated tubulin (green) and F-actin (phalloidin; red) (lower panels) in p27 KO MEFs immersed in a 3D collagen I matrix (control) in the presence of C3-exoenzyme (2 ng/ml) or Y27632 (10 μM), as indicated. Typical images acquired by confocal microscopy are shown.

teins and exert crucial functions in cellular signaling and protein trafficking (42). In their report the authors demonstrated that both the intracellular accumulation of lipid rafts in suspended cells and their relocalization to the plasma membrane following cell adhesion to ECM require the integrity of MT (1). These observations are in accord with the notion that MTs provide a polarized intracellular network that allows organelle and protein movement throughout the cell, serving as tracks for intracellular vesicular trafficking that, in turn, are required for complex cellular functions, such as migration, as well as division and adhesion. To verify whether an altered intracellular vesicular trafficking could be implicated in the morphological and motile phenotypes observed in p27 KO cells, we set up the same assay aimed to monitor internalization of lipid rafts in these cells. We used the CTxB as a fluorescent marker for these membrane microdomains (1), both in suspended cells and following adhesion to ECM. Fibroblasts of different genotypes were labeled with CTxB while still adherent in the culture dish, then they were detached and held in suspension for different times, and finally the cells were cytospun and observed with a confocal microscope. Under these conditions, CTxB locates at the cell membrane during the labeling procedure and then during suspension starts to be internalized and moves to a distinct perinuclear region around the MTOC (1). After 5 min of suspension WT fibroblasts still retain CTxB labeling at the surface, while in the same time frame many p27 KO cells already exhibit perinuclear accumulation of the toxin (Fig. 5A). This sharp difference attenuates with time, tending to disappear after 60 min of suspension (Fig. 5B). If cells are held in suspension for 60 min and then replated on FN-coated dishes, CTxB moves again toward the cellular periphery in a time-dependent manner (1). When performing this kind of experiment and fixing the cells after 30 min of adhesion to FN, again we could clearly notice a more rapid redistribution of the CTxB to the cell membrane in 3T3 p27 KO fibroblasts compared to WT cells. Membrane relocalization of CTxB in DKO fibroblasts resembled the timing seen in WT cells, suggesting that the p27/stathmin ratio plays a role also in this process (Fig. 5C and D). Stable reintroduction of p27 in p27 KO cells produced a cellular response very similar to that of WT cells, thus confirming that the observed effects were specifically due to the absence of p27 (Fig. 5A to D). Similarly, the analysis of primary MEFs showed that the majority of CTxB-labeled lipid rafts were still spread in the cytoplasm of WT and DKO fibroblasts during the first 60 min of adhesion, while they had already reached the cell membrane in p27 KO cells (Fig. 5E and F).

These results were then confirmed using video time-lapse microscopy analysis. For these experiments, cells were prelabeled with CTxB and observed while in suspension to analyze the rate of perinuclear accumulation of the rafts. When WT cells were tested in this type of assay, only a few cells displayed perinuclear accumulation of CTxB (Fig. 6A, upper panels; see also Video S4 in the supplemental material), while most of the p27 KO cells had already internalized the toxin (Fig. 6A, middle panels; see also Video S5). Importantly, when p27 KO cells were held in suspension in the presence of 10 or 100 nm paclitaxes (Fig. 6A and B; see also Video S6), the internalization of CTxB was completely prevented, confirming that the

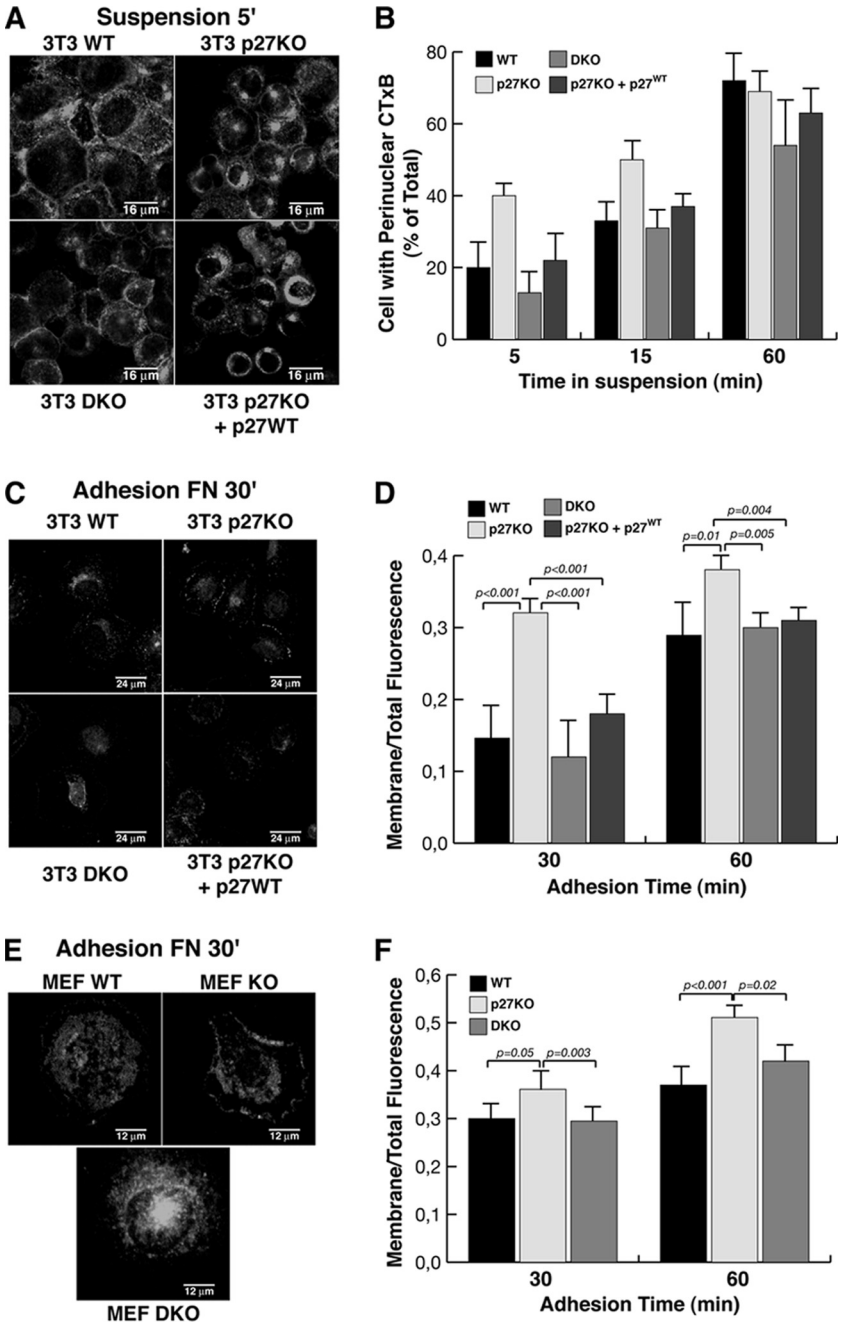

FIG. 5. p27 KO fibroblasts display altered vesicular trafficking. (A) Confocal microscopy of WT, p27 KO, DKO, and p27 KO 3T3 fibroblasts stably reexpressing p27 and labeled with CTxB (green) to visualize lipid rafts. Cells were labeled for 15 min at 4°C and then detached and kept in suspension for 5 min to allow the internalization of labeled lipid rafts. White arrowheads indicate cells with perinuclear accumulation of labeled lipid rafts. Typical images of cytospun cells are shown. (B) Graphical presentation of the results from the experiments shown in panel A, based on the number cells positive for perinuclear accumulation of labeled lipid rafts at the indicated times of suspension, expressed as a percentage of total counted cells. The results represent the means of two different experiments, in which at least 100 cells for each cell population and for each time point were counted. (C) The same experiment as in panel A, except cells were kept in suspension for 60 min to allow complete internalization of labeled lipid rafts (CTxB; red) and then adhered to FN-coated coverslips for 30 min to monitor lipid raft relocalization to the plasma membrane. Nuclei were counterstained with Sytox Green (green). (D) Graphical presentation of the ratios between the fluorescence present at the membrane level and the total fluorescence of the cell, from the experiments described for panel C. The results represent the means of two different experiments in which at least 20 cells for each cell population and for each time point were analyzed using the Leica LAS software. (E) Same experiment as in panel C, except that primary MEFs were used. (F) Graphical presentation of the ratios between the fluorescence present at the membrane level and the total fluorescence of the cell, from experiments described for panel E. The results represent the means of two different experiments, in which at least 20 cells for each cell population and for each time point were analyzed using the Leica LAS software.

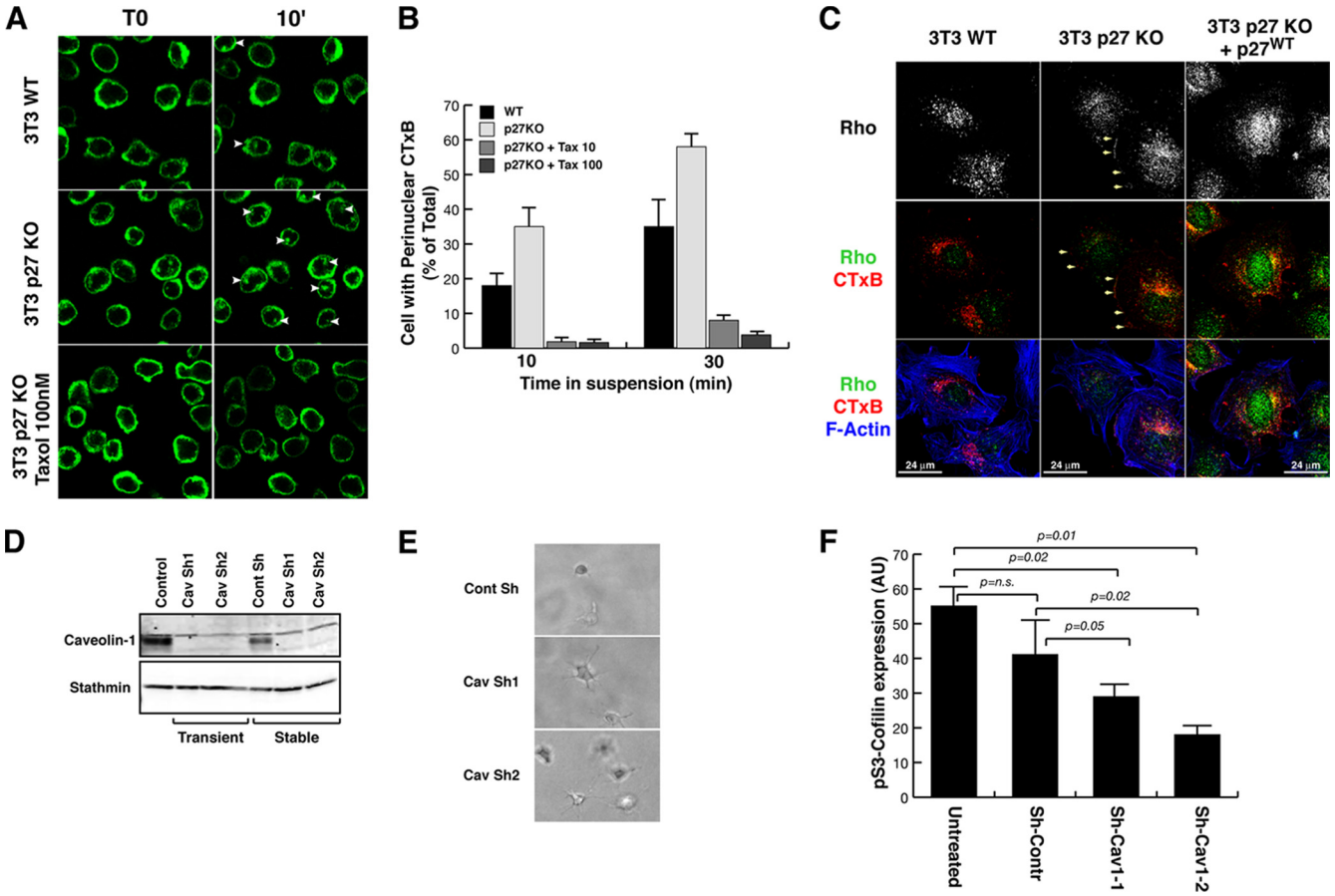

FIG. 6. Altered vesicular trafficking of p27 KO fibroblasts relies on impaired MT stability. (A) Confocal images from time-lapse microscopy analysis of WT and p27 KO 3T3 fibroblasts. Cells prelabeled with CTxB (green) were detached and layered onto poly-HEMA-coated coverslips to impede adhesion and observed while in suspension for up to 10 min. In the bottom panels p27 KO 3T3 fibroblasts were pretreated for 2 h with 100 nM paclitaxel and then labeled and treated as described above, always in the presence of paclitaxel. White arrowheads indicate cells with perinuclear accumulation of labeled lipid rafts. (B) Graphical presentation of the results shown in panel A based on the number of cells positive for perinuclear accumulation of labeled lipid rafts at the indicated times of suspension, expressed as a percentage of total counted cells. The results represent the means of three different experiments in which at least 100 cells for each cell population and at each time point were counted. (C) Immunofluorescence analysis of RhoA (green), F-actin (phalloidin, pseudocolored in blue), and lipid rafts (CTxB; red) in WT p27 KO 3T3 fibroblats and p27 KO 3T3 fibroblasts stably reexpressing p27. Cells were labeled with CTxB, detached, held in suspension for 60 min, allowed to adhere to FN-coated coverslips for 30 min, and then fixed. In the upper panels RhoA localization is shown in gray. Yellow arrows indicate membrane localization of CTxB and RhoA. (D) Western blot analysis of caveolin-1 expression in p27 KO 3T3 cells transduced with lentiviral vectors encoding for nontarget control-specific or two different caveolin-1-specific shRNAs, as indicated. (E) Phase-contrast microscopy images of p27 KO 3T3 cells stably transduced with two different shRNAs against caveolin 1 (middle and bottom panels) or a nontarget control shRNA (top panel), included in the 3D collagen I matrix for 5 h. A typical image is shown, and a 20× objective was used. (F) Graphical presentation of IF analyses for pSer3 cofilin in p27 KO cells transduced or not with nontarget control shRNA or shRNAs against caveolin-1 and included in the 3D collagen I matrix. Results are expressed as arbitrary units, using Leica LAS software for the computational analysis of mean fluorescent level/cell and represent the means of three independent experiments in which the fluorescence of at least 20 cells has been calculated.

faster internalization of lipid rafts in the p27 KO cells relied on the decreased MT stability observed in these cells.

Then, we verified whether this accelerated lipid raft trafficking is a mechanism that also functions during cell-ECM contact and whether it is linked to the higher RhoA activity measured in the absence of p27. To this aim, cells were labeled with CTxB, held in suspension to allow for perinulear accumulation, and then adhered to FN and fixed for immunofluorescence analysis. The data showed that, similar to what occurs with CTxB, increased levels of RhoA protein were localized at the cell periphery in p27 KO cells respect to WT fibroblasts (Fig. 6C). Again this effect was abrogated by reintroduction of p27 in p27 KO cells (Fig. 6C) and in p27/stathmin DKO MEFs (see Fig. S8C), confirming that this is a p27-dependent phenotype due to variation of stathmin activity.

These results suggest that accelerated vesicular trafficking is linked to increased RhoA activity in p27 KO cells in contact with ECM, and we hypothesized that this mechanism could also account for their rounded cell shape and amoeboid-like motility in 3D contexts.

Thus, we speculated that impinging on vesicular trafficking of p27 KO cells should affect their shape and motility in 3D. Recently, it has been proposed that, following cell detachment, lipid rafts are internalized through caveolae in a process that requires both dynamin-2 activity and phosphorylation of caveolin-1 (13). Either a dominant negative dynamin-2 con-

struct or knockdown of caveolin 1 completely blocked the internalization process (13). Similarly, we used two different approaches to affect the lipid raft trafficking of p27 null cells. First, we treated cells with Dynasore, a cell-permeant small molecule that specifically inhibits the GTPase activity of dynamin (27), in experiments of cell inclusion in 3D collagen I gels. Video time-lapse microscopy demonstrated p27 KO fibroblasts acquire their typical rounded shape coupled with the amoeboid motility when included in 3D collagen I (see Video S7 in the supplemental material), but in the presence of Dynasore they formed long protrusions and were no longer able to move (see Video S8). Second, we knocked down caveolin-1 expression in p27 null cells (Fig. 6D) by using lentiviral transduction of specific shRNAs. Also, caveolin-1 silencing profoundly altered cellular morphology and motility of p27 KO cells in a 3D context, as demonstrated by phase-contrast observations and video time-lapse microscopy of cells immersed in collagen I (Fig. 6E). Caveolin-1-silenced cells were no longer able to properly move in a 3D collagen I matrix and started to form long cellular protrusions (Fig. 6E; see also Videos S9 and S10 in the supplemental material), compared to p27 KO control cells, thus recapitulating the effects observed after treatment with Dynasore. Then, to substantiate the idea that RhoA is the downstream effector of this pathway, we evaluated the phosphorylation of Ser3 cofilin in p27 KO fibroblasts silenced by caveolin. Cells were included in a 3D collagen I matrix, and immunofluorescence analysis was performed against pSer3 cofilin. Computational analysis of the mean fluorescence level/cell demonstrated that caveolin-1-silenced cells displayed significantly lower staining for pSer3 cofilin than control p27 KO cells (Fig. 6F), thus supporting the role of lipid raft recycling in the Rho hyperactivation observed in p27 KO cells.

DISCUSSION

The coordinated regulation of cell proliferation and migration and its disorders underlie several physiological and pathological processes, such as embryogenesis, organ development, and cancer metastasis. In all of these processes p27 and/or stathmin has been implicated. In an experimental model of vascular injury in mice, Nabel and coworkers reported that absence of p27 accelerated wound healing closure (8), while impairment of stathmin function resulted in an opposite effect in the same assay (22). Accordingly, in an experimental model of stroke in mice (18) and in xenograft models of human tumors (34, 40), overexpression of p27 determined an impaired neovasculature formation. On the other hand, stathmin ablation in *Drosophila melanogaster* impairs border cell, germ cell, and neuronal cell motility (9, 35). Interestingly, while acute alterations of both stathmin (19) and p27 (20) levels in mice affect neuronal motility, neither stathmin nor p27 null mice display apparent anatomical defects in the organization of the peripheral or central nervous systems (16, 41), suggesting that compensatory mechanisms must exist to allow for proper mouse development. However, the molecular characterization of how p27 and stathmin regulate cell motility was incomplete to date. Here, we tried to fill this gap by demonstrating that p27 and stathmin act in concert in modulating RhoA activity, via the modification of MT stability. Other reports have described how p27 modulates RhoA activity by direct association, but this has been proven only in overexpression model systems (6). Interestingly, we recently demonstrated in a v-*src* transformation model that absence of p27 is linked to an increase in RhoA activity, which is then associated with an augmented metastatic potential (5). This phenotype could be suppressed by reexpression of p27 protein but only if the domain responsible for the interaction with stathmin were retained (5), thus supporting our present conclusions. Whether p27-RhoA direct binding is also present under physiological conditions and whether it is stathmin dependent will need further work and could be important to understand.

Cell cycle regulatory proteins already have been implicated in the control of MT stability, and emerging evidence suggests that this process, conserved during evolution, represents a cellular expedient to coordinate proliferation and motility. The most compelling proof comes from yeast, where cyclin-dependent kinase 1 (CDK1) translocates into the cytoplasm after the completion of mitosis to control MT stability, thus contributing to guidance of bud formation (25, 28). In higher eukaryotic model systems, CDK1 and cyclin D1 have been proposed to take part in the regulation of cell motility (23, 24, 29), at least in part through the modulation of p27 localization/activity. Interestingly, cyclin D1 regulation of cell motility also has been associated with increased expression of stathmin (24), a known CDK1 substrate (30). Although the regulation of cell motility by p27 seems to be via a CDK-independent mechanism (2, 5, 6, 31), further work will be necessary to address this point exhaustively.

The observation that p27 may regulate RhoA activity via vesicular trafficking describes an unexpected convergence of distinct lines of evidence. In fact, the roles reported so far for p27 are pleiotropic and sometimes contrasting: it has been described as either an inhibitor or stimulator of motility (2, 5, 6, 18, 31) and tumor suppressor or oncogene (4, 7, 15, 16, 33). Interestingly, stathmin activity also has been linked to vesicular trafficking regulation in T-helper cells, where it contributes to the control of interleukin-4 receptor recycling (44), thus independently confirming our findings. The data reported by Tanaka et al. for T cells (44) and by others for neurons (46), along with our present and previous observations (2, 3), suggest that the activation of stathmin and that of small GTPases are strongly connected. It is conceivable that, at least during the first phases of cell-ECM contact, a regulatory loop exists in order to maintain a balanced activity of these different players, with increased stathmin activity leading to increased RhoA activation and increased RhoA activation stabilizing the MT network after cell adhesion (36). Since RhoA activity also influences Rac-dependent signaling (reviewed in reference 10), this could eventually control the stathmin MT-destabilizing function via phosphorylation of its inhibitory serine residues (44, 46, 48). In this manner the correct balance between small GTPase activity and MT stability following cell contact with ECM could be simply maintained. One link between activation of RhoA and MT depolymerization has been proposed (11, 21) following treatment with high doses of nocodazole, resulting in the activation of RhoA by the release of the RhoA-GEF GEF-H1 from depolymerized MTs. Yet, the role of GEF-H1 under physiological conditions is still unclear. However, veri-

fying whether the p27-stathmin interaction regulates the availability of GEF-H1 is worth considering.

The results of our study demonstrate that fine-tuning of MT stability can profoundly affect intracellular vesicle recycling and eventually results in alteration of cell morphology and motility. Although we did not directly prove that also in 3D setting p27 KO cells display faster lipid raft trafficking, our data suggest that their recycling is critical not only for integrin-mediated signaling pathway modulation in anchorage-dependent cell growth (13) but also for the acquirement of mesenchymal shape and motility in 3D matrices. Since the p27-stathmin interaction controls cell plasticity and motility in 3D matrices also in transformed cells (2, 3, 5, 40), possibly via the modulation of Rho activity (5), the mechanism described here may be relevant for several aspects of cancer cell behavior, thus highlighting possible future interventions.

In conclusion, we describe here a totally new p27 function which eventually controls cellular morphology and motility and opens new perspectives to the understanding of p27 loss phenotypes and its role in tumor progression.

ACKNOWLEDGMENTS

This work was supported by Associazione Italiana Ricerca sul Cancro to G.B. S.B. is a recipient of a Federazione Italiana Ricerca Sul Cancro fellowship.

We declare that we have no competing financial interests.

REFERENCES

1. **Balasubramanian, N., D. W. Scott, J. D. Castle, J. E. Casanova, and M. A. Schwartz.** 2007. Arf6 and microtubules in adhesion-dependent trafficking of lipid rafts. Nat. Cell Biol. **12:**1381–1391.
2. **Baldassarre, G., B. Belletti, M. S. Nicoloso, M. Schiappacassi, A. Vecchione, P. Spessotto, A. Morrione, V. Canzonieri, and A. Colombatti.** 2005. p27(Kip1)-stathmin interaction influences sarcoma cell migration and invasion. Cancer Cell **7:**51–63.
3. **Belletti, B., M. S. Nicoloso, M. Schiappacassi, S. Berton, F. Lovat, K. Wolf, V. Canzonieri, S. D'Andrea, A. Zucchetto, P. Friedl, A. Colombatti, and G. Baldassarre.** 2008. Stathmin activity influences sarcoma cell shape, motility, and metastatic potential. Mol. Biol. Cell **19:**2003–2013.
4. **Belletti, B., M. S. Nicoloso, M. Schiappacassi, E. Chimienti, S. Berton, F. Lovat, A. Colombatti, and G. Baldassarre.** 2005. p27(kip1) functional regulation in human cancer: a potential target for therapeutic designs. Curr. Med. Chem. **12:**1589–1605.
5. **Berton, S., B. Belletti, K. Wolf, V. Canzonieri, F. Lovat, A. Vecchione, A. Colombatti, P. Friedl, and G. Baldassarre.** 2009. The tumor suppressor functions of p27(kip1) include control of the mesenchymal/amoeboid transition. Mol. Cell. Biol. **29:**5031–5045.
6. **Besson, A., M. Gurian-West, A. Schmidt, A. Hall, and J. M. Roberts.** 2004. p27Kip1 modulates cell migration through the regulation of RhoA activation. Genes Dev. **18:**862–876.
7. **Besson, A., H. C. Hwang,S. Cicero, S. L. Donovan, M. Gurian-West, D. Johnson, B. E. Clurman, M. A. Dyer, and J. M. Roberts.** 2007. Discovery of an oncogenic activity in p27Kip1 that causes stem cell expansion and a multiple tumor phenotype. Genes Dev. **21:**1731–1746.
8. **Boehm, M., M. Olive, A. L. True, M. F. Crook, H. San, X. Qu, and E. G. Nabel.** 2004. Bone marrow-derived immune cells regulate vascular disease through a p27(Kip1)-dependent mechanism. J. Clin. Invest. **114:**419–426.
9. **Borghese, L., G. Fletcher, J. Mathieu, A. Atzberger, W. C. Eades, R. L. Cagan, and P. Rorth.** 2006. Systematic analysis of the transcriptional switch inducing migration of border cells. Dev. Cell **10:**497–508.
10. **Burridge, K., and K. Wennerberg.** 2004. Rho and Rac take center stage. Cell **116:**167–179.
11. **Chang, Y. C., P. Nalbant, J. Birkenfeld, Z. F. Chang, and G. M. Bokoch.** 2008. GEF-H1 couples nocodazole-induced microtubule disassembly to cell contractility via RhoA. Mol. Biol. Cell **19:**2147–2153.
12. **Degani, S., F. Balzac, M. Brancaccio, S. Guazzone, S. F. Retta, L. Silengo, A. Eva, and G. Tarone.** 2002. The integrin cytoplasmic domain-associated protein ICAP-1 binds and regulates Rho family GTPases during cell spreading. J. Cell Biol. **156:**277–287.
13. **del Pozo, M. A., N. Balasubramanian, N. B. Alderson, W. B. Kiosses, A. Grande-García, R. G. Anderson, and M. A. Schwartz.** 2005. Phospho-caveolin-1 mediates integrin-regulated membrane domain internalization. Nat. Cell Biol. **7:**901–908.
14. **Etienne-Manneville, S.** 2004. Actin and microtubules in cell motility: which one is in control? Traffic **5:**470–477.
15. **Fero, M. L., E. Randel, K. E. Gurley, J. M. Roberts, and C. J. Kemp.** 1998. The murine gene p27Kip1 is haplo-insufficient for tumour suppression. Nature **396:**177–180.
16. **Fero, M. L., M. Rivkin, M. Tasch, P. Porter, C. E. Carow, E. Firpo, K. Polyak, L. H. Tsai, V. Broudy, R. M. Perlmutter, K. Kaushansky, and J. M. Roberts.** 1996. A syndrome of multiorgan hyperplasia with features of gigantism, tumorigenesis, and female sterility in p27(Kip1)-deficient mice. Cell **85:**733–744.
17. **Friedl, P., and K. Wolf.** 2003. Tumour-cell invasion and migration: diversity and escape mechanisms. Nat. Rev. Cancer **3:**362–374.
18. **Goukassian, D., A. Diez-Juan, T. Asahara, P. Schratzberger, M. Silver, T. Murayama, J. M. Isner, and V. Andrés.** 2001. Overexpression of p27(Kip1) by doxycycline-regulated adenoviral vectors inhibits endothelial cell proliferation and migration and impairs angiogenesis. FASEB J. **15:**1877–1885.
19. **Jin, K., X. O. Mao, B. Cottrell, B. Schilling, L. Xie, R. H. Row, Y. Sun, A. Peel, J. Childs, G. Gendeh, B. W. Gibson, and D. A. Greenberg.** 2004. Proteomic and immunochemical characterization of a role for Stathmin in adult neurogenesis. FASEB J. **18:**287–299.
20. **Kawauchi, T., K. Chihama, Y. Nabeshima, and M. Hoshino.** 2006. Cdk5 phosphorylates and stabilizes p27kip1 contributing to actin organization and cortical neuronal migration. Nat. Cell Biol. **8:**17–26.
21. **Krendel, M., F. T. Zenke, and G. M. Bokoch.** 2002. Nucleotide exchange factor GEF-H1 mediates cross-talk between microtubules and the actin cytoskeleton. Nat. Cell Biol. **4:**294–301.
22. **Langenickel, T. H., M. Olive, M. Boehm, H. San, M. F. Crook, and E. G. Nabel.** 2008. KIS protects against adverse vascular remodeling by opposing Stathmin-mediated VSMC migration in mice. J. Clin. Invest. **118:**3848–3859.
23. **Li, Z., X. Jiao, C. Wang, X. Ju, Y. Lu, L. Yuan, M. P. Lisanti, S. Katiyar, and R. G. Pestell.** 2006. Cyclin D1 induction of cellular migration requires p27(KIP1). Cancer Res. **66:**9986–9994.
24. **Li, Z., C. Wang, X. Jiao, S. Katiyar, M. C. Casimiro, G. C. Prendergast, M. J. Powell, and R. G. Pestell.** 2008. Alternate cyclin D1 mRNA splicing modulates p27KIP1 binding and cell migration. J. Biol. Chem. **283:**7007–7015.
25. **Liakopoulos, D., J. Kusch, S. Grava, J. Vogel, and Y. Barral.** 2003. Asymmetric loading of Kar9 onto spindle poles and microtubules ensures proper spindle alignment. Cell **112:**561–574.
26. **Maaser, K., K. Wolf, C. E. Klein, B. Niggemann, K. S. Zänker, E. B. Brocker, and P. Friedl.** 1999. Functional hierarchy of simultaneously expressed adhesion receptors: integrin $\alpha 2\beta 1$ but not CD44 mediates MV3 melanoma cell migration and matrix reorganization within three-dimensional hyaluronan-containing collagen matrices. Mol. Biol. Cell **10:**3067–3079.
27. **Macia, E., M. Ehrlich, R. Massol, E. Boucrot, C. Brunner, and T. Kirchhausen.** 2006. Dynasore, a cell-permeable inhibitor of dynamin. Dev. Cell **10:**839–850.
28. **Maekawa, H., T. Usui, M. Knop, and E. Schiebel.** 2003. Yeast Cdk1 translocates to the plus end of cytoplasmic microtubules to regulate bud cortex interactions. EMBO J. **22:**438–449.
29. **Manes, T., D. Q. Zheng, S. Tognin, A. S. Woodard, P. C. Marchisio, and L. R. Languino.** 2003. $\alpha v\beta 3$ integrin expression up-regulates cdc2, which modulates cell migration. J. Cell Biol. **161:**817–826.
30. **Marklund, U., O. Osterman, H. Melander, A. Bergh, and M. Gullberg.** 1994. The phenotype of a "Cdc2 kinase target site-deficient" mutant of oncoprotein 18 reveals a role of this protein in cell cycle control. J. Biol. Chem. **269:**30626–30635.
31. **McAllister, S. S., M. Becker-Hapak, G. Pintucci, M. Pagano, and S. F. Dowdy.** 2003. Novel p27(kip1) C-terminal scatter domain mediates Rac-dependent cell migration independent of cell cycle arrest functions. Mol. Cell. Biol. **23:**216–228.
32. **Moffat, J., D. A. Grueneberg, X. Yang, S. Y. Kim, A. M. Kloepfer, G. Hinkle, B. Piqani, T. M. Eisenhaure, B. Luo, J. K. Grenier, A. E. Carpenter, S. Y. Foo, S. A. Stewart, B. R. Stockwell, N. Hacohen, W. C. Hahn, E. S. Lander, D. M. Sabatini, and D. E. Root.** 2006. A lentiviral RNAi library for human and mouse genes applied to an arrayed viral high-content screen. Cell **124:**1283–1298.
33. **Muraoka, R. S., A. E. Lenferink, B. Law, E. Hamilton, D. M. Brantley, L. R. Roebuck, and C. L. Arteaga.** 2002. ErbB2/Neu-induced, cyclin D1-dependent transformation is accelerated in p27-haploinsufficient mammary epithelial cells but impaired in p27-null cells. Mol. Cell. Biol. **22:**2204–2219.
34. **Nickeleit, I., S. Zender, F. Sasse, R. Geffers, G. Brandes, I. Sorensen, H. Steinmetz, S. Kubicka, T. Carlomagno, D. Menche, I. Gutgemann, J. Buer, A. Gossler, M. P. Manns, M. Kalesse, R. Frank, and N. P. Malek.** 2008. Argyrin A reveals a critical role for the tumor suppressor protein p27(kip1) in mediating antitumor activities in response to proteasome inhibition. Cancer Cell **8:**23–35.
35. **Ozon, S., A. Guichet, O. Gavet, S. Roth, and A. Sobel.** 2002. Drosophila Stathmin: a microtubule-destabilizing factor involved in nervous system formation. Mol. Biol. Cell **13:**698–710.
36. **Palazzo, A. F., C. H. Eng, D. D. Schlaepfer, E. E. Marcantonio, and G. G. Gundersen.** 2004. Localized stabilization of microtubules by integrin- and FAK-facilitated Rho signaling. Science **303:**836–839.

37. **Sahai, E., R. Garcia-Medina, J. Pouysségur, and E. Vial.** 2007. Smurf1 regulates tumor cell plasticity and motility through degradation of RhoA leading to localized inhibition of contractility. J. Cell Biol. **176:**35–42.
38. **Sahai, E., and C. J. Marshall.** 2003. Differing modes of tumour cell invasion have distinct requirements for Rho/ROCK signalling and extracellular proteolysis. Nat. Cell Biol. **5:**711–719.
39. **Sahai, E.** 2007. Illuminating the metastatic process. Nat. Rev. Cancer **7:**737–749.
40. **Schiappacassi, M., F. Lovat, V. Canzonieri, B. Belletti, S. Berton, D. Di Stefano, A. Vecchione, A. Colombatti, and G. Baldassarre.** 2008. p27Kip1 expression inhibits glioblastoma growth, invasion, and tumor-induced neoangiogenesis. Mol. Cancer Ther. **7:**1164–1175.
41. **Schubart, U. K., J. Yu, J. A. Amat, Z. Wang, M. K. Hoffmann, and W. Edelmann.** 1996. Normal development of mice lacking metablastin (P19), a phosphoprotein implicated in cell cycle regulation. J. Biol. Chem. **271:**14062–14066.
42. **Shima, T., S. Nada, and M. Okada.** 2003. Transmembrane phosphoprotein Cbp senses cell adhesion signaling mediated by Src family kinase in lipid rafts. Proc. Natl. Acad. Sci. U. S. A. **100:**14897–14902.
43. **Siegrist, S. E., and C. Q. Doe.** 2007. Microtubule-induced cortical cell polarity. Genes Dev. **21:**483–496.
44. **Tanaka, Y., S. Hamano, K. Gotoh, Y. Murata, Y. Kunisaki, A. Nishikimi, R. Takii, M. Kawaguchi, A. Inayoshi, S. Masuko, K. Himeno, T. Sasazuki, and Y. Fukui.** 2007. T helper type 2 differentiation and intracellular trafficking of the interleukin 4 receptor-alpha subunit controlled by the Rac activator Dock2. Nat. Immunol. **8:**1067–1075.
45. **Vial, E., E. Sahai, and C. J. Marshall.** 2003. ERK-MAPK signaling coordinately regulates Rac1 and RhoA for tumor cell motility. Cancer Cell **4:**67–79.
46. **Watabe-Uchida, M., K. A. John, J. A. Janas, S. E. Newey, and L. Van Aelst.** 2006. The Rac activator DOCK7 regulates neuronal polarity through local phosphorylation of Stathmin/Op18. Neuron **51:**727–739.
47. **Watanabe, T., J. Noritake, and K. Kaibuchi.** 2005. Regulation of microtubules in cell migration. Trends Cell Biol. **15:**76–83.
48. **Wittmann, T., G. M. Bokoch, and C. M. Waterman-Storer.** 2004. Regulation of microtubule destabilizing activity of Op18/Stathmin downstream of Rac1. J. Biol. Chem. **279:**6196–6203.
49. **Wolf, K., I. Mazo, H. Leung, K. Engelke, U. H. von Andrian, E. I. Deryugina, A. Y. Strongin, E. B. Brocker, and P. Friedl.** 2003. Compensation mechanism in tumor cell migration: mesenchymal-amoeboid transition after blocking of pericellular proteolysis. J. Cell Biol. **160:**267–277.
50. **Yamada, K. M., and E. Cukierman.** 2007. Modeling tissue morphogenesis and cancer in 3D. Cell **130:**601–610.